Dual-energy computed-tomography-based discrimination between basic calcium phosphate and calcium pyrophosphate crystal deposition *in vivo*

Tristan Pascart (iD), Guillaume Falgayrac, Laurène Norberciak, Clément Lalanne, Julie Legrand, Eric Houvenagel, Hang-Korng Ea, Fabio Becce* (iD) and Jean-François Budzik*

Abstract

Background: Dual-energy computed tomography (DECT) is being considered as a non-invasive diagnostic and characterization tool in calcium crystal-associated arthropathies. Our objective was to assess the potential of DECT in distinguishing between basic calcium phosphate (BCP) and calcium pyrophosphate (CPP) crystal deposition in and around joints *in vivo*.

Methods: A total of 13 patients with calcific periarthritis and 11 patients with crystal-proven CPPD were recruited prospectively to undergo DECT scans. Samples harvested from BCP and CPP calcification types were analyzed using Raman spectroscopy and validated against synthetic crystals. Regions of interest were placed in BCP and CPP calcifications, and the following DECT attenuation parameters were obtained: CT numbers (HU) at 80 and 140 kV, dual-energy index (DEI), electron density (Rho), and effective atomic number (Z_{eff}). These DECT attenuation parameters were compared and validated against crystal calibration phantoms at two known equal concentrations. Receiver operating characteristic (ROC) curves were plotted to determine the highest accuracy thresholds for DEI and Z_{eff}.

Results: Raman spectroscopy enabled chemical fingerprinting of BCP and CPP crystals both *in vitro* and *in vivo*. DECT was able to distinguish between HA and CPP in crystal calibration phantoms at two known equal concentrations, most notably by DEI ($200\,mg/cm^3$: 0.037 ± 0 *versus* 0.034 ± 0, $p = 0.008$) and Z_{eff} ($200\,mg/cm^3$: 9.4 ± 0 *versus* 9.3 ± 0, $p = 0.01$) analysis. Likewise, BCP calcifications had significantly higher DEI (0.041 ± 0.005 *versus* 0.034 ± 0.005, $p = 0.008$) and Z_{eff} (9.5 ± 0.2 *versus* 9.3 ± 0.2, $p = 0.03$) than CPP crystal deposits with comparable CT numbers in patients. With an area under the ROC curve of 0.83 [best threshold value = 0.039, sensitivity = 90.9% (81.8, 97.7%), specificity = 64.6% (50.0, 64.6%)], DEI was the best parameter in distinguishing between BCP and CPP crystal depositions.

Conclusion: DECT can help distinguish between crystal-proven BCP and CPP calcification types *in vivo* and, thus, aid in the diagnosis of challenging clinical cases, and in the characterization of CPP and BCP crystal deposition occurring in osteoarthritis.

Correspondence to:
Tristan Pascart
Department of
Rheumatology, Lille
Catholic Hospitals,
Saint-Philibert Hospital,
University of Lille, Rue
du Grand But, Lomme,
F-59160, France

EA 4490, PMOI,
Physiopathologie des
Maladies Osseuses
Inflammatoires, University
of Lille, Lille, France
pascart.tristan@ghicl.net

Guillaume Falgayrac
EA 4490, PMOI,
Physiopathologie des
Maladies Osseuses
Inflammatoires, University
of Lille, Lille, France

Laurène Norberciak
Department of Medical
Research, Biostatistics,
Lille Catholic Hospitals,
University of Lille, Lomme,
France

Clément Lalanne
Department of Orthopaedic
Surgery, Lille Catholic
Hospitals, University of
Lille, Lomme, France

Julie Legrand
Department of Diagnostic
and Interventional
Radiology, Lille Catholic
Hospitals, University of
Lille, Lomme, France

Eric Houvenagel
Department of
Rheumatology, Lille
Catholic Hospitals,
University of Lille, Lomme,
France

Hang-Korng Ea
Department of
Rheumatology, Hôpital
Lariboisière, AP-HP, Paris,
France

INSERM U1132, Université
Paris Diderot, Paris,
France

Fabio Becce
Department of Diagnostic
and Interventional
Radiology, Lausanne
University Hospital and
University of Lausanne,
Lausanne, Switzerland

Introduction

Basic calcium phosphate (BCP) and calcium pyrophosphate (CPP) are the two most common types of calcium-containing crystals associated with musculoskeletal syndromes. Although BCP are typically encountered in periarticular flares (calcific periarthritis), CPP crystals are found in acute gout mimicking (formerly "pseudogout") or chronic arthritis [clustered under the umbrella term CPP deposition (CPPD) disease].[1,2] In calcific tendinitis,

François Budzik
EA 4490, PMOI,
Physiopathologie des
Maladies Osseuses
Inflammatoires, University
of Lille, Lille, France

Department of Diagnostic
and Interventional
Radiology, Lille Catholic
Hospitals, University of
Lille, Lomme, France

*F. Becce and J.-F. Budzik
contributed equally to this
work.

the most commonly involved BCP crystals are carbonate apatites, which are chemically similar to calcium hydroxyapatite (HA) present in bone tissues.[3] Both BCP and CPP crystal deposits can be observed and induce arthritis in the axial skeleton, and identifying the spinal calcium crystals of interest remains a diagnostic challenge. Furthermore, BCP and CPP crystal deposition coexist in human hyaline and fibrocartilage during the course of osteoarthritis (OA), yet their respective pathogenic roles, if any, remain to be determined.[4]

While CPP crystals can be identified by synovial fluid analysis, though with moderate sensitivity and reliability,[5] BCP crystals cannot be found using standard of care polarized light microscopy because of their small size, which requires advanced diagnostic methods such as scanning electron microscopy.[1] The chemical fingerprint of BCP crystals can be determined using vibrational techniques such as Raman spectroscopy, which is however not yet widely available in clinical practice.[6,7] Imaging is therefore often pivotal in diagnosing calcium crystal-associated musculoskeletal diseases, provided that spatial resolution and the amount of crystals deposited permit their detection.[8,9] Although both ultrasound and conventional CT are more sensitive than plain radiography, none of these techniques allows definite characterization of the types of calcium-containing crystals involved. Dual-energy computed tomography (DECT), owing to its material decomposition and tissue characterization capabilities, has the potential to distinguish between BCP and CPP crystal deposits.[10] A recent proof-of-concept study showed that DECT was able to discriminate meniscal CPP deposits from HA in subchondral and trabecular bone *in vivo*,[11] most recently followed by its first clinical translation in the non-invasive characterization of knee intra-articular mineralization.[12] These findings were supported by a pilot clinical study on DECT sensitivity for CPPD,[13] and a further *ex vivo* study using multi-energy photon-counting CT.[14] However, the question of whether clinically available DECT is able to distinguish articular CPP deposits from HA-containing articular and/or periarticular calcifications *in vivo* still needs answering.

Therefore, the main objective of this study was to assess the potential of DECT in distinguishing between BCP and CPP crystal deposition in joints and periarticular soft tissues, by non-invasive analysis and characterization of their DECT attenuation biochemical signatures.

Materials and methods

Synthetic crystals and calibration phantoms
Synthetic pure HA and CPP crystals were used as reference to determine the marker bands (peaks) characterizing the Raman spectra of each calcium crystal type. In addition, CT calibration phantoms of HA and CPP crystals at two known equal concentrations (50 and 200 mg/cm^3) were manufactured (Computerized Imaging Reference Systems, Norfolk, VA, USA) from synthetic crystals (Sigma-Aldrich, St. Louis, MO, USA) suspended in a resin mimicking fat tissue with no chemical element having significant photoelectric absorption. These 5-mm-diameter crystal calibration phantoms were inserted into a custom 10-cm-diameter cylindrical polyethylene holder filled with water, thereby mimicking soft tissue attenuation of joints in DECT scans. No bone tissue was included in the phantom.

Patients
A total of 13 consecutive patients (10 women) aged 57 ± 18 years, with a mean symptom duration of 8.7 ± 8.8 months for calcific periarthritis/BCP crystal deposition disease, were prospectively enrolled in this institutional review board-approved study (Institut National des Données de Santé, protocol 3114300419). All patients presented with typical manifestations and flares of calcific periarthritis/tendinitis, with presence of BCP crystal deposition on plain radiographs. They were recruited to undergo DECT scans of their calcifications/affected joints (8 type I, 4 type II, and 1 type III calcifications according to Gärtner and Heyer[15]), 11/13 (84.6%) of which were located at the shoulder. Six patients, who underwent surgical or image-guided percutaneous needle aspiration and lavage (barbotage) of their BCP-type calcifications, consented to donate the extracted calcium-containing material for Raman spectroscopic analysis. A total of 11 patients (7 women) aged 81 ± 9 years with both chondrocalcinosis on knee DECT scans and crystal-proven CPPD in synovial fluid analysis were retrospectively selected as controls.[11]

DECT protocol
DECT scans were performed using a single-source dual-energy CT system (Somatom Definition Edge; Siemens Healthineers, Erlangen, Germany). Data were acquired using the helical acquisition mode with the following settings: tube

potentials, 80 and 140 kV; quality reference tube current-time products at 80 and 140 kV, 150–215 and 37–47 mAs, respectively; beam collimation, 128×0.6 mm²; pitch, 0.7; overall volume CT dose indexes, 2.9–4.8 mGy. Images were then reconstructed as follows: section thickness/overlap, 0.75/0.25 mm; field of view, 250×250 mm², yielding in-plane pixel sizes of 0.49×0.49 mm²; both smooth (B30f) and sharp (B70f) kernels.

Image analysis

DECT datasets were post-processed and analyzed on a dedicated workstation using a proprietary DE software (syngo.CT DE Rho/Z; Siemens Healthineers). A rheumatologist experienced in crystal-associated arthropathies placed regions of interest (ROIs; circular in calibration phantoms *versus* polygonal in tendons and menisci) encompassing HA/BCP and CPP phantoms/calcifications on five consecutive CT sections, while paying particular attention to avoiding partial volume effects. For BCP-type calcifications in patients, two sets of ROIs were obtained: the first in the central portion (highest density on grayscale CT images), and the second in a peripheral portion (lower density) of periarticular calcifications. For each ROI, five DECT attenuation parameters were obtained: CT numbers (in Hounsfield unit, HU) at low (80 kV) and high (140 kV) tube potentials, dual-energy index (DEI), electron density (Rho), and effective atomic number (Z_{eff}).

Raman spectroscopy

Spectra were obtained using a Raman microspectrometer (LabRAM HR800; Horiba Jobin Yvon, Palaiseau, France), with a spectral range set to 300–1700 cm⁻¹ and a resolution of 4 cm⁻¹. Raman spectra were post-processed using a dedicated software (LabSpec; Horiba). Samples harvested from BCP-type calcifications and synthetic HA and CPP crystals were mounted on a slide. Five Raman spectra per sample were acquired with an average acquisition time of 60 s ($\times$ 4 repeated acquisitions $\times$ 5 spectra = 20 min per sample). Furthermore, five spectra of CPP crystals from the synovial fluid of a single CPPD patient were obtained using the same settings, to provide a control spectrum of biological CPP crystals. The characteristic marker bands of both synthetic and biological Raman spectra were noted.[16]

Statistical analysis

Data were analyzed using R (version 3.4.2; R Foundation for Statistical Computing, Vienna, Austria). Qualitative variables are reported as numbers (%), while quantitative variables as mean ± standard deviation (SD). Synthetic HA and CPP calibration phantoms were compared using Wilcoxon–Mann–Whitney test. Patient characteristics between BCP and CPPD groups were compared using Wilcoxon–Mann–Whitney or Fisher exact tests, where appropriate. Given repeated measurements on each subject, the different sets of ROIs in BCP and CPPD patients were compared using linear mixed models, considering patients as random effects, and age as fixed effect when adjusting for confounders. Briefly, model validation was evaluated graphically using residuals (normality and homoscedasticity). When conditions were not satisfied even after log-transformation, permutation tests were implemented to estimate p-values with 5000 permutations.[11] Receiver operating characteristic (ROC) curves were plotted to determine the highest accuracy thresholds for DEI and Z_{eff} in distinguishing between BCP and CPP crystal deposition. Statistical significance was set at $p < 0.05$.

Results

Raman spectroscopy enables chemical fingerprinting of BCP and CPP crystal deposition *in vivo*

Raman spectra of synthetic pure HA and CPP crystals were readily distinguished because they exhibited characteristic marker bands (peaks) representative of material-specific chemical bonds (Figure 1). The synthetic HA spectrum was characterized by a high-intensity $\nu_1 PO_4$ band at 961 cm⁻¹, and lower intensity bands at 1075, 1046, 1027, 607, 589, 577, 445, and 429 cm⁻¹. In contrast, the synthetic CPP spectrum was typified by a high-intensity $\nu_1 PO_4$ band at 1,048 cm⁻¹, and lower intensity bands at 1181, 1121, 1112, 1079, 797, and 752 cm⁻¹. A group of lower-intensity bands was also observed in the ~450–650 cm⁻¹ spectral region. All six BCP-type calcifications obtained by image-guided percutaneous needle aspiration and lavage or surgical procedures exhibited the same characteristic marker bands as those of synthetic HA crystals, with additional bands in the ~1000–1800 cm⁻¹ spectral region, which are typical of organic compounds, particularly collagen (Figure 1). The spectrum of biological CPP
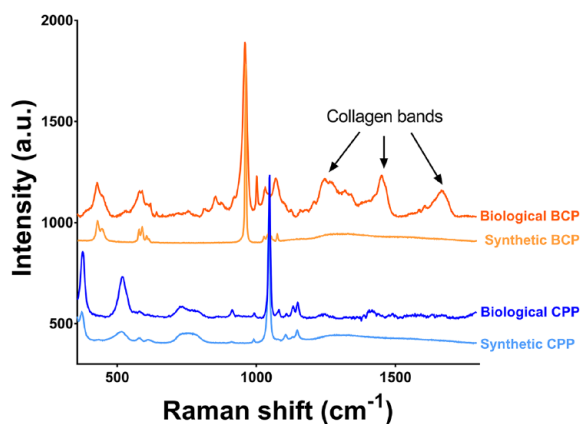
Figure 1. Average Raman spectra, with characteristic marker bands, of both synthetic and biological basic calcium phosphate (BCP), most notably calcium hydroxyapatite (HA) and carbonate apatite, and calcium pyrophosphate (CPP) crystals.

crystals exhibited the same characteristic marker bands compared with synthetic CPP crystals, without any additional band (Figure 1).

DECT can distinguish between synthetic HA and CPP crystal calibration phantoms at equal concentrations

CT numbers at low (80 kV) and high (140 kV) tube potentials, DEI, Rho, and Z_{eff} of HA and CPP crystal calibration phantoms at two known equal concentrations are reported in Table 1.

At both 50 and 200 mg/cm³, HA differed significantly from CPP crystal phantoms in terms of CT numbers at 80 kV (200 mg/cm³: 344 ± 4 *versus* 335 ± 7, $p = 0.03$), DEI (200 mg/cm³: 0.037 ± 0.001 *versus* 0.034 ± 0.001, $p = 0.008$),

and Z_{eff} (200 mg/cm³: 9.4 ± 0 *versus* 9.3 ± 0, $p = 0.01$), due to higher photoelectric absorption for HA crystals (Figure 2). In contrast and as expected per our study design, Rho (200 mg/cm³: 141 ± 5 *versus* 149 ± 6, $p = 0.06$) and CT numbers at 140 kV (200 mg/cm³: 248 ± 5 *versus* 248 ± 8, p = 0.75) were both comparable between HA and CPP crystal phantoms, regardless of concentration (Figure 2).

DECT can moderately distinguish BCP from CPP calcifications in vivo

CT numbers at 80 and 140 kV, DEI, Rho, and Z_{eff} of periarticular BCP (both central and peripheral portions) and articular CPP calcifications in patients are reported in Table 2.

The central portion of BCP calcifications differed significantly from their peripheral portion and CPP crystal deposits, for all five DECT attenuation parameters considered ($p < 0.0001$, Figure 3). When comparing the peripheral portion (lower density on grayscale CT images) of BCP with CPP crystal deposits, CT numbers at 80 and 140 kV (425 ± 66 *versus* 341 ± 58, $p = 0.02$; and 313 ± 63 *versus* 252 ± 44, $p = 0.03$, respectively), DEI (0.041 ± 0.005 *versus* 0.034 ± 0.005, $p = 0.008$), and Z_{eff} (9.5 ± 0.2 *versus* 9.3 ± 0.2, $p = 0.03$) were all significantly higher in BCP patients, while Rho (216 ± 54 *versus* 167 ± 33, $p = 0.06$) was comparable between the two calcification types (Figure 3). With an area under the ROC curve (AUC) of 0.83 [best threshold value = 0.039, sensitivity (95% confidence intervals) = 90.9% (81.8, 97.7%), specificity = 64.6% (50.0, 64.6%)], DEI was the most accurate DECT parameter in distinguishing between BCP and CPP crystal deposition in and around joints,

Table 1. Dual-energy computed tomography (DECT) attenuation parameters of synthetic calcium hydroxyapatite (HA) and calcium pyrophosphate (CPP) crystal calibration phantoms at two known equal concentrations (50 and 200 mg/cm³).

	HA 50	CPP 50	*p*-value	HA 200	CPP 200	*p*-value
CT numbers 80 kV (HU)	86 ± 3	70 ± 4	0.01	344 ± 4	335 ± 7	0.03
CT numbers 140 kV (HU)	80 ± 4	74 ± 4	0.06	248 ± 5	248 ± 8	0.75
DEI	0.003 ± 0.002	−0.002 ± 0.001	0.008	0.037 ± 0.001	0.034 ± 0.001	0.008
Rho	79 ± 8	79 ± 3	0.84	141 ± 5	149 ± 6	0.06
Z_{eff}	7.5 ± 0.1	7.3 ± 0	0.03	9.4 ± 0	9.3 ± 0	0.01

DEI, dual-energy index; HU, Hounsfield unit; Rho, electron density; Z_{eff}, effective atomic number.
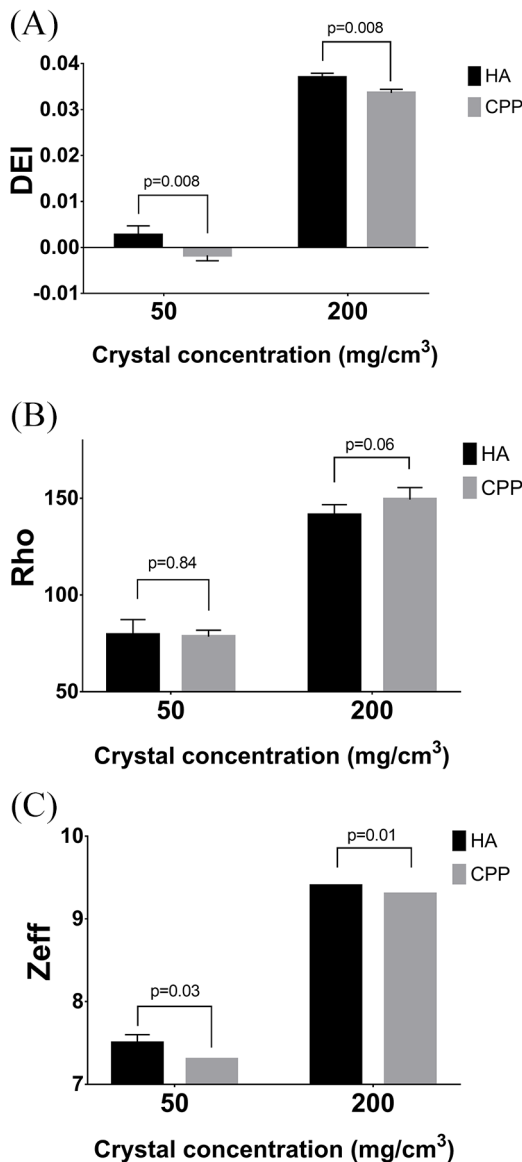
Figure 2. Comparison of dual-energy computed tomography (DECT) attenuation parameters between synthetic calcium hydroxyapatite (HA) and calcium pyrophosphate (CPP) crystal calibration phantoms at two known equal concentrations (50 and 200 mg/cm^3): (A) dual-energy index (DEI), (B) electron density (Rho), and (C) effective atomic number (Z_{eff}).

followed by Z_{eff} with an AUC of 0.80 [best threshold value = 9.42, sensitivity = 77.3% (63.6, 88.6%), specificity = 75.0% (62.5, 87.5%); Figure 4].

Discussion

Our *in vitro*/phantom study shows that DECT can distinguish between synthetic HA and CPP crystals at two different equal concentrations, most notably by DEI and Z_{eff} analysis. We found that the same held true *in vivo* between crystal-proven BCP and CPP crystal deposits in two different patient groups with typical clinical characteristics for either BCP or CPP crystal-associated musculoskeletal diseases, though with moderate accuracy (high sensitivity but low specificity with DEI, and moderate sensitivity and specificity with Z_{eff}). This study further confirms the chemical fingerprinting capabilities of Raman spectroscopy through identification of characteristic marker bands of BCP and CPP crystals.

At similar densities/concentrations, distinguishing between BCP and CPP calcifications using plain radiography or conventional CT can remain challenging because of overlapping grayscale attenuation values/CT numbers. While CPP deposits are typically found in the knee, wrist (triangular fibrocartilage complex), and/or pubic symphysis, and BCP aggregates around the shoulder,[17] the anatomical location, size and shape of calcium crystal deposits can also overlap, and different calcification types may coexist including in the knee[12,14] and cervical spine. Despite the recent establishment of OMERACT definitions for CPPD identification by ultrasound, their reliability still highly depends on the anatomical location.[18] In contrast, DECT provides additional information that can aid in differentiating BCP from CPP-containing crystal deposits. BCP and CPP crystals have specific chemical compositions as shown by the Raman spectroscopic analysis. By enabling the decomposition of Compton scattering (related to Rho numbers) and photoelectric absorption (related to Z_{eff} numbers), DECT provides the ability to discriminate tissue materials (i.e. molecular signature).[10,11] While typical BCP calcifications are denser than CPP crystal deposits, a qualitative feature which is already identified by conventional CT,[17] decomposing the information obtained at dual X-ray energies, either through two distinct X-ray beams or dual-layer detectors, is necessary to discriminate the two calcification types. Indeed, a difference in photoelectric absorption leads to higher Z_{eff} and DEI for BCP than CPP crystals, even at similar densities/concentrations.[11] While our patients were purposefully selected for their typical clinical and radiological presentations, distinguishing between BCP and CPP crystals is yet another challenge in cases where anatomical location and density can be equivocal such as in the cervical spine. Although far from perfect, the diagnostic

Table 2. Dual-energy computed tomography (DECT) attenuation parameters of periarticular basic calcium phosphate (BCP, both central and peripheral portions) and articular calcium pyrophosphate (CPP) in patients.

	BCP central	BCP peripheral	CPP
CT numbers 80 kV (HU)	707 ± 115	425 ± 66	341 ± 58
CT numbers 140 kV (HU)	506 ± 85	313 ± 63	252 ± 44
DEI	0.062 ± 0.007	0.041 ± 0.005	0.034 ± 0.005
Rho	333 ± 66	216 ± 54	167 ± 33
Z_{eff}	10.4 ± 0.3	9.5 ± 0.2	9.3 ± 0.2

DEI, dual-energy index; HU, = Hounsfield unit; Rho, electron density; Z_{eff}, effective atomic number.
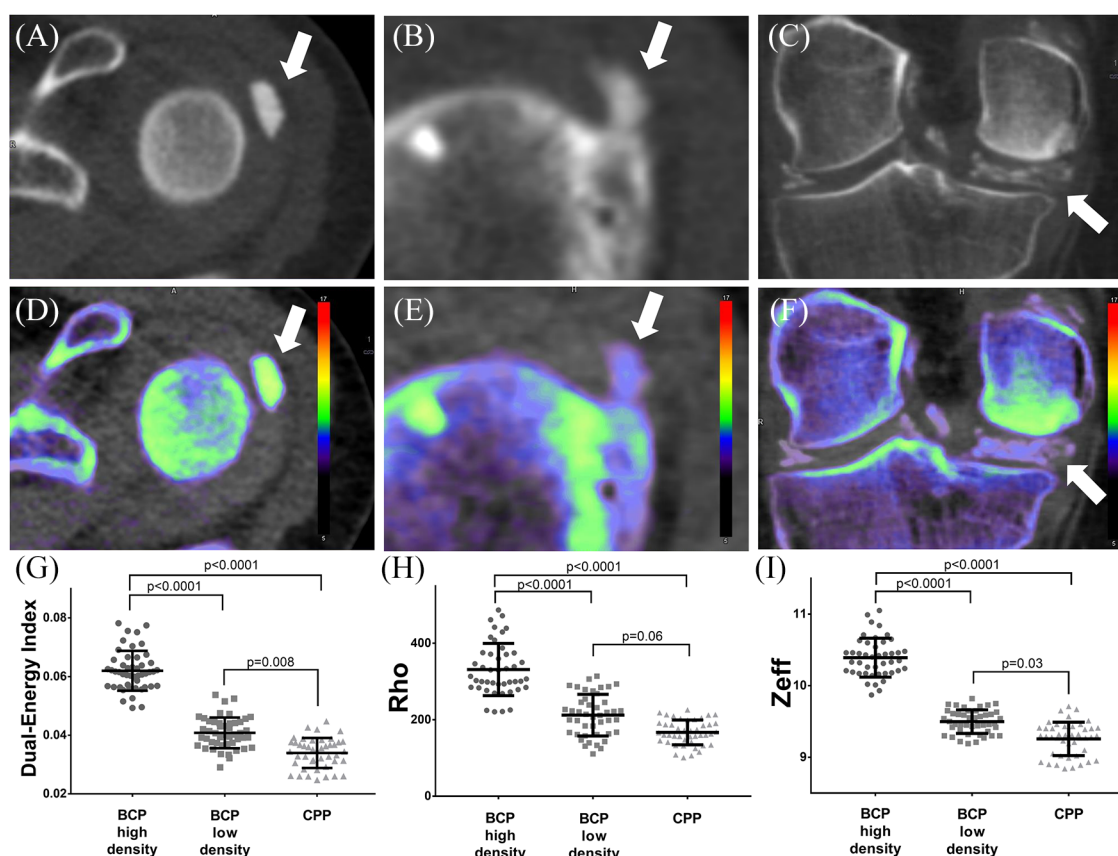

Figure 3. Dual-energy computed tomography (DECT) scans (A, D, shoulder, central/highest-density portion; B, E, shoulder, peripheral/lower-density portion; C, F, knee) and DECT attenuation parameters (G–I) of basic calcium phosphate (BCP) compared with calcium pyrophosphate (CPP) calcification types. Conventional grayscale CT images (A–C) with corresponding color-coded Rho/Z overlay DECT images (D–F) post-processed using proprietary Rho/Z software. Comparison of dual-energy index (DEI, G), electron density (Rho, H), and effective atomic number (Z_{eff}, I) in regions of interest encompassing BCP (both central and peripheral portions) and CPP calcifications.

performance of DEI with a sensitivity of over 90% remains interesting in the prospect of discriminating between BCP and CPP calcifications in such challenging clinical scenarios. Furthermore, considering that DECT's ability to differentiate BCP from CPP aggregates is independent of the anatomical location or shape of calcifications, our results should therefore be translatable to more
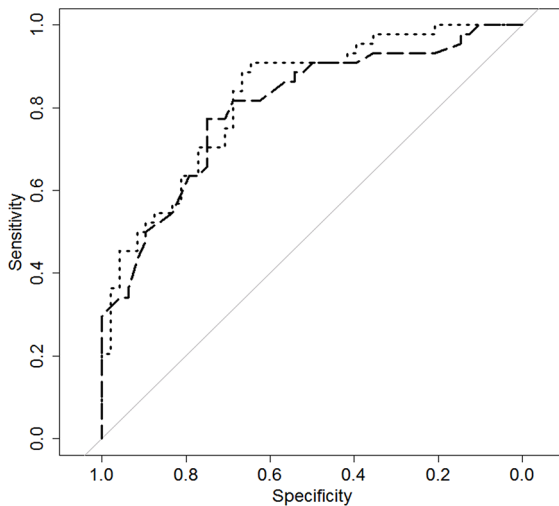
Figure 4. Receiver operating characteristic (ROC) curves show the accuracy of dual-energy index (DEI, dotted line) and effective atomic number (Z_{eff}, dashed line) in distinguishing between basic calcium phosphate (BCP) and calcium pyrophosphate (CPP) crystal deposition in and around joints.

complex clinical cases. Further studies including BCP calcifications with naturally lower density (especially type III or calcifications in their resorptive phase) would aid in confirming these initial results.

Combining Raman spectroscopy and DECT for the study of calcium-containing crystal deposition in musculoskeletal diseases could meet the current clinical and research needs for definite calcium crystal characterization, quantification, and mapping.[19] Our study confirms that the bands of interest from Raman spectra of the different calcium-containing crystals are readily distinguished, especially through a different shift in the $\nu_1 PO_4$ band. Although Raman spectroscopy is for the time being still not widely available in routine clinical practice, a successful attempt was made to develop a point-of-care device the size of a shoebox.[7] Pursuing the development of such clinically available devices would provide an easy-to-use reference standard for calcium-crystal discrimination on biological samples (calcifications and/or synovial fluid aspirates). Taking a step further, Raman spectroscopy might be considered for *in vivo* analysis as it was experimented in gout on the first metatarsophalangeal joint, with the technical limitation for calcium-crystal deposition inherent to their deeper location from the body surface.[20] DECT is less accurate than Raman spectroscopy for the characterization of

calcium-containing crystals and currently limited by spatial resolution constraints, but offers the possibility of determining the general 3D distribution and quantifying these crystal deposits over time, as this is already feasible with monosodium urate deposition in gout.[21,22]

A potential major clinical application of the discriminative capability of DECT is the study of the various types of cartilage calcifications occurring in OA and their potential roles as active players in cartilage damage *versus* innocent bystanders.[4,23] *Ex vivo* studies have shown that the coexistence of CPP and BCP crystals deposited in OA joints is a very common feature.[24] In contrast to the typical BCP tendon calcifications included in this study where crystals are densely packed, the local density of BCP crystals in OA joints resembles that of CPP crystals. Exploring these lower-density intra-articular calcifications with DECT could provide insights into the relative proportion of each calcium crystal, as higher DEI and Z_{eff} numbers would suggest a higher proportion of BCP crystals.[11] The DECT-based analysis method demonstrated here has just been applied to the first clinical case of non-invasive characterization of knee intra-articular mineralization.[12]

We acknowledge the following study limitations. First, the small number of patients may have underestimated the Rho difference (related to density/concentration) between BCP and CPP calcifications *in vivo*. However, the substantial overlap in DECT Rho numbers implies that this difference would not be clinically meaningful. Another limitation is inherent to the DECT technology itself. Both spatial resolution (minimum ~250 µm) and the use of energy-integrating detectors rather than energy-resolving photon-counting detectors only allows for the detection of differences that are numerically small and difficult to translate into clinical practice.[25] With increased spatial resolution (down to ~100 µm) and the possibility of combining attenuation properties of numerous energy bins (up to eight energy bins), upcoming multi-energy photon-counting CT systems will certainly add to the discriminative abilities of CT systems for calcium crystal deposition.[8,14,26,27] Finally, the diagnostic performance of DECT-based thresholds for DEI and Z_{eff} reported here might be overestimated because they were applied to a clinically typical exploratory patient cohort from which they were determined. Indeed, both CPP and BCP patients deliberately presented typical clinical and radiological characteristics for this proof-of-concept DECT

study. Further diagnostic accuracy studies are needed in different, more challenging clinical settings to reassess the diagnostic performance of these initial DECT-based threshold values.

Conclusion

In conclusion, DECT can aid in distinguishing between crystal-proven BCP and CPP calcification types *in vivo* with moderate accuracy, by non-invasively analyzing and characterizing their DECT attenuation biochemical signatures. The emergence of multi-energy photon-counting CT with enhanced diagnostic capabilities, in particular higher spatial and contrast resolutions, opens up new horizons for the non-invasive detection, characterization, quantification, and mapping of calcium crystal deposition. This is essential not only to determine the calcium crystal of interest in challenging clinical scenarios when conventional imaging techniques and features fail to identify the culprit calcium crystal, but also to gain a better understanding and deeper insights into the pathogenic role that these crystals may play in the various calcium crystal-associated musculoskeletal diseases, including in OA.

ORCID iDs
Tristan Pascart (iD) https://orcid.org/0000-0002-8395-826X

Fabio Becce (iD) https://orcid.org/0000-0001-8444-8504

References

1. McCarthy GM and Dunne A. Calcium crystal deposition diseases - beyond gout. *Nat Rev Rheumatol* 2018; 14: 592–602.

2. Rosenthal AK and Ryan LM. Calcium pyrophosphate deposition disease. *N Engl J Med* 2016; 374: 2575–2584.

3. Hamada J, Tamai K, Ono W, *et al*. Does the nature of deposited basic calcium phosphate crystals determine clinical course in calcific periarthritis of the shoulder? *J Rheumatol* 2006; 33: 326–332.

4. Fuerst M, Bertrand J, Lammers L, *et al*. Calcification of articular cartilage in human osteoarthritis. *Arthritis Rheum* 2009; 60: 2694–2703.

5. Andres M, Vela P, Jovani V, *et al*. Most needle-shaped calcium pyrophosphate crystals lack birefringence. *Rheumatology (Oxford)* 2019; 58: 1095–1098.

6. Chiou HJ, Hung SC, Lin SY, *et al*. Correlations among mineral components, progressive calcification process and clinical symptoms of calcific tendonitis. *Rheumatology (Oxford)* 2010; 49: 548–555.

7. Li B, Singer NG, Yeni YN, *et al*. A point-of-care Raman Spectroscopy-based device for the diagnosis of Gout and Pseudogout: comparison with the clinical standard microscopy. *Arthritis Rheumatol* 2016; 68: 1751–1757.

8. Becce F, Viry A, Stamp LK, *et al*.; MARS Collaboration. Winds of change in imaging of calcium crystal deposition diseases. *Joint Bone Spine* 2019; 86: 665–668.

9. Filippou G, Pascart T and Iagnocco A. Utility of ultrasound and dual energy CT in crystal disease diagnosis and management. *Curr Rheumatol Rep* 2020; 22: 15.

10. Omoumi P, Becce F, Racine D, *et al*. Dual-energy CT: basic principles, technical approaches, and applications in musculoskeletal imaging (Part 1). *Semin Musculoskelet Radiol* 2015; 19: 431–437.

11. Pascart T, Norberciak L, Legrand J, *et al*. Dual-energy computed tomography in calcium pyrophosphate deposition: initial clinical experience. *Osteoarthritis Cartilage* 2019; 27: 1309–1314.

12. Collinot JA, Pascart T, Budzik JF, *et al*. Non-invasive characterization of intra-articular mineralization using dual-energy computed tomography. *Rheumatology (Oxford)* 2020. Epub ahead of print. DOI: 10.1093/rheumatology/keaa231.

13. Tedeschi SK, Solomon DH, Yoshida K, *et al*. A prospective study of dual-energy CT scanning, US and X-ray in acute calcium pyrophosphate crystal arthritis. *Rheumatology (Oxford)* 2020; 59: 900–903.

14. Stamp LK, Anderson NG, Becce F, *et al.* Clinical utility of multi-energy spectral photon-counting CT in crystal arthritis. *Arthritis Rheumatol* 2019; 71(7):1158–1162.

15. Gärtner J and Heyer A. [Calcific tendinitis of the shoulder]. *Orthopade* 1995; 24: 284–302.

16. Penel G, Delfosse C, Descamps M, *et al.* Composition of bone and apatitic biomaterials as revealed by intravital Raman microspectroscopy. *Bone* 2005; 36: 893–901.

17. Freire V, Moser TP and Lepage-Saucier M. Radiological identification and analysis of soft tissue musculoskeletal calcifications. *Insights Imaging* 2018; 9: 477–492.

18. Filippou G, Scire CA, Adinolfi A, *et al.* Identification of calcium pyrophosphate deposition disease (CPPD) by ultrasound: reliability of the OMERACT definitions in an extended set of joints-an international multiobserver study by the OMERACT calcium pyrophosphate deposition disease ultrasound subtask force. *Ann Rheum Dis* 2018; 77: 1194–1199.

19. Abhishek A, Neogi T, Choi H, *et al.* Unmet needs and the path forward in joint disease associated with calcium pyrophosphate crystal deposition. *Arthritis Rheumatol* 2018; 70: 1182–1191.

20. Abhishek A, Curran DJ, Bilwani F, *et al.* In vivo detection of monosodium urate crystal deposits by Raman spectroscopy-a pilot study. *Rheumatology (Oxford)* 2016; 55: 379–380.

21. Pascart T, Grandjean A, Norberciak L, *et al.* Ultrasonography and dual-energy computed tomography provide different quantification of urate burden in gout: results from a cross-sectional study. *Arthritis Res Ther* 2017; 19: 171.

22. Richette P, Doherty M, Pascual E, *et al.* 2018 updated European League Against Rheumatism evidence-based recommendations for the diagnosis of gout. *Ann Rheum Dis* 2020; 79: 31–38.

23. Ea HK, Nguyen C, Bazin D, *et al.* Articular cartilage calcification in osteoarthritis: insights into crystal-induced stress. *Arthritis Rheum* 2011; 63: 10–18.

24. Nguyen C, Bazin D, Daudon M, *et al.* Revisiting spatial distribution and biochemical composition of calcium-containing crystals in human osteoarthritic articular cartilage. *Arthritis Res Ther* 2013; 15: R103.

25. Willemink MJ, Persson M, Pourmorteza A, *et al.* Photon-counting CT: technical principles and clinical prospects. *Radiology* 2018; 289: 293–312.

26. Kirkbride TE, Raja AY, Muller K, *et al.* Discrimination between calcium hydroxyapatite and calcium oxalate using multienergy spectral photon-counting CT. *AJR Am J Roentgenol* 2017; 209: 1088–1092.

27. Simard M, Panta RK, Bell ST, *et al.* Quantitative imaging performance of MARS spectral photon-counting CT for radiotherapy. *Med Phys*. Epub ahead of print 24 April 2020.

Visit SAGE journals online
journals.sagepub.com/
home/tab

§SAGE journals